Cytotherapy, 2017; 19: 61–74

International Society for Cellular Therapy
ISCT®

CrossMark

Human mesenchymal stromal cells undergo apoptosis and fragmentation after intravenous application in immune-competent mice

JOHANNES LEIBACHER[1], KATRIN DAUBER[1], SABRINA EHSER[1], VERONIKA BRIXNER[1], KATARINA KOLLAR[1], ANJA VOGEL[1], GABI SPOHN[1], RICHARD SCHÄFER[1], ERHARD SEIFRIED[1] & REINHARD HENSCHLER[1,2]

[1]*Institute of Transfusion Medicine and Immune Hematology, German Red Cross Blood Donor Service, University of Frankfurt, UK, and* [2]*Blood Transfusion Services Zurich and Grisons, Swiss Red Cross, Switzerland*

Abstract

Background aims. The biodistribution of human MSCs after systemic delivery is incompletely understood. We investigated the changes in cell size and cell surface markers of human MSCs after intravenous (IV) injection in immune competent mice. *Methods.* Male human MSCs were labeled with fluorescent vital dye PKH67 and tracked after IV administration in C57/BL6 mice. MSCs were tracked in blood and different murine tissues by human *SRY* gene quantitative polymerase chain reaction (qPCR) analysis, flow cytometry and fluorescence microscopy. Calibrated microbeads were used to track the size of transplanted MSCs. *Results.* The majority of injected MSCs were detected by qPCR in the lungs 5 min after transplantation, whereas <0.1% were detected in other tissues over 24 h. Flow cytometric and fluorescence microscopic analysis indicated that MSCs continuously decreased in size after transplantation and underwent fragmentation. The majority of PKH^+ MSCs and their fragments were found in lungs and liver. PKH^+ MSCs rapidly became positive for annexin V, propidium iodide and calreticulin, indicating loss of cell integrity. In addition, PKH^+ fragments co-stained with antibodies against C3b, F4/80 and/or GR-1 indicating opsonization. Preincubation of MSCs in hyperosmolaric hydroxyethyl starch (HyperHAES) decreased MSCs size before transplantation, delayed the loss of viability markers and increased the frequency of traceable MSCs up to 24 h after transplantation. *Conclusions.* PKH67 labeled MSCs are fragmented after IV injection in mice, acquire apoptotic and phagocytic cell markers and accumulate in the lungs and liver.

Key Words: *biodistribution, hyperosmolaric media, intravenous application, mouse, mesenchymal stromal cells, PKH67*

Introduction

Mesenchymal stromal cells (MSCs) are a population of progenitor cells that can be isolated from different tissues, adapt spindle-shaped morphology in culture and be expanded or differentiated into different mesenchymal cells types [1,2]. *Ex vivo* expanded MSCs express a variety of markers including CD73, CD90 and CD105 but do not express hematopoietic cell antigens including CD11b, CD14, CD19, CD34, CD45, CD79a and HLA-DR (<5%) [2]. Additional markers such as CD44, CD140b, CD146, CD271, CD340 and CD349 have been described to allow prospective isolation of MSC populations with more primitive characteristics and enrichment of colony-forming unit fibroblasts [3–5]. Human MSCs can be expanded *in vitro* for up to 40–50 population doublings and do not show significant telomerase activity [6–8]. Extensive *in vitro* expansion of MSCs has been associated with increased production of matrix metalloproteinase inhibitors, resulting in impaired interaction of MSCs with ECM and lower migration capacity [9,10]. Moreover, a decrease in expression of adhesion molecules, loss of chemokine receptors, general change in morphology and subsequent lack of chemotactic response have been related to a reduced the ability of expanded MSCs to migrate to sites of inflammation [11–13]. After systemic administration, culture-expanded MSCs were generally seen to accumulate in the lungs and only at very low frequencies in other tissues, and they could generally not be traced for longer than 3–4 days [10–12,14].

Thus up to date, the *in vivo* fate of the majority of transplanted MSCs and their quantitative biodistribution is unclear. MSCs have been shown to interact with platelets [15], but their cellular or molecular target structures in the blood circulation remain to be resolved. To better

Correspondence: Dr. phil. nat. **Johannes Leibacher**, Institut für Transfusionsmedizin und Immunhämatologie Frankfurt am Main, Sandhofstr.1, DE, 60528 Frankfurt, UK. E-mail: Johannes_leibacher@web.de

(Received 4 March 2016; accepted 13 September 2016)

ISSN 1465-3249
http://dx.doi.org/10.1016/j.jcyt.2016.09.010

understand the biodistribution and the fate of MSCs after intravenous (IV) administration, we traced human MSCs in immunocompetent mice early after transplantation using a human-specific DNA probe and the PKH67 vital fluorescence marker. We used calibrated microbeads and flow cytometry to determine the size of the transplanted MSCs and assessed expression of apoptosis markers. Furthermore, we preincubated MSCs in hyperosmolaric hydroxyethyl starch (HyperHAES) to decrease the cell diameter before transplantation and to improve the survival of transplanted MSCs.

Methods

Isolation and cultivation of bone marrow–derived human MSCs

MSCs were obtained from healthy bone marrow donors after informed consent in accordance with the Declaration of Helsinki and according to a vote of the local ethics committee (vote 102/03). The bone marrow aspirates were anticoagulated with 500 IU/mL heparin and conducted through a three-way filter-system (Fenwal/Fresenius). MSCs were removed from the filters by retrograde flushing and collected in 50-mL polypropylene tubes. The low-density fraction was prepared using Biocoll separation solution (density 1.077 g/mL, Biochrome) and centrifugation at 800*g* for 15 min, following collection of the interphase layer. Cells were seeded in T75 plastic flasks at a density of $1–3 \times 10^6$ cells/cm^2 in low-glucose Dulbecco's Modified Eagle's Medium (DMEM; PAA) supplemented with 20% tested fetal calf serum (FCS; PAN Biotech) and 1% penicillin/streptomycin/amphotericin B (Gibco/Life Technologies), then incubated at 37°C and 5% CO_2. After 3–5 days, non-adherent cells were removed, and the remaining cells were cultured for 7–10 days until cell density reached 75% confluency. The uniform spindle-shaped cells were passaged by 0.05% Trypsin-ethylenediaminetetraacetic acid (Gibco/Life Technologies) and culture medium was changed twice a week. MSC populations were grown until passage 6. For MSCs detachment before transplantation, StemPro Accutase (Gibco/Life Technologies) was used instead of 0.05% trypsin.

Colony formation assay

Clonogenic potential was determined with MSCs at early passage after 1×10^6 mononuclear cells per flask were seeded in normal culture condition media. On day 14, cells were washed twice with Dulbecco's phosphate-buffered saline (D-PBS; Gibco/Life Technologies GmbH) and stained with 0.5% crystal violet solution (Sigma Aldrich, Steinheim, Germany) for 30 min at room temperature. Cells were washed with D-PBS and rinsed with tap water. Remaining fluids were removed by drying flask in an upright position on a paper towel. Colony-forming unit fibroblasts count was enumerated with a minimum of 50 cells in close contact. Pictures were taken using microscope Olympus IX71.

Mesenchymal differentiation and staining

Human MSCs were plated at 2.4×10^4/well in DMEM/20% fetal bovine serum until 75% confluency was reached using standard culture conditions. Medium was then changed to NH-adipocyte differentiation medium for 3 weeks with complete medium changes twice a week (Miltenyi). Staining of triglycerides and lipids was performed by 0.33% oil red O staining solution (Sigma Aldrich) for 1 h at room temperature. For osteogenic differentiation, 100% confluent MSCs were grown in StemMacs-Osteo differentiation media (Miltenyi). Osteocyte differentiation was demonstrated by 1-h incubation in a 2% silver nitrate solution (Sigma Aldrich) at room temperature under UV light. After washing, cells were incubated in 2.5% sodium thiosulfate solution (Sigma Aldrich) for 5 min under constant agitation. Cells were washed with D-PBS and incubated for 1 min with 1% neutral red solution (Sigma Aldrich). For chondrocytic differentiation, 5×10^5 MSCs were seeded into a 15-mL tube with NH-chrondo differentiation medium (Miltenyi). Cells formed clusters after 24–48 h at 37°C and 5% CO_2 and received weekly full medium changes. After 3 weeks, the cell cluster at the bottom of the tube was covered with 65°C paraffin (Sigma Aldrich), and 4-µm sections were prepared onto glass slides using a Leica RM 2235 Microtome (Leica Biosystems). Slides were incubated for 50 min in a 56°C furnace and treated twice with 99.8% Xylol for 5 min. Sections were fixed in methanol at –20°C, and the remaining water was removed by serial dilution in ethanol. One percent toluidine blue (Sigma Aldrich) in 50% isopropanol was used to stain cells for 30 min. All photos were taken using microscope Olympus IX71.

Phalloidin A staining

Cells ($0.1–1 \times 10^6$) were resuspended in either D-PBS (Gibco/Life Technologies) or HyperHAES (Fresenius Kabi) and fixed for 10 min with 4% paraformaldehyde (Sigma Aldrich) at room temperature. Cells were washed 3 × with either D-PBS or HyperHAES and Phalloidin A (diluted 1:100) was added per well. The cell samples were incubated for 1 h at room temperature under constant agitation following analysis using Olympus IX 71 microscope.

PKH67 staining

PKH67 (Sigma Aldrich) staining was performed in single cell suspensions containing $0.6–1 \times 10^7$ MSCs, which had been washed once in serum-free DMEM.

The staining was performed according to the manufacturers' instructions. Briefly, PKH was added and cells were mixed by constant inversion of the tube for 5 min. Unbound PKH67 molecules were then blocked by adding 100% FCS (1:1), and the suspension was centrifuged for 5 min at 1600*g*. The supernatant was carefully aspirated, and the cells were resuspended in culture medium for immediate use.

Staining for mitochondrial membrane potential

For the staining procedure, 1×10^6 cells were prepared in a 1.5-mL Eppendorf tube in a volume of 500-μL culture medium. Tetramethyl-rhodamine-methylester perchlorate (TMRM) staining solution (1 μmol/L in dimethyl sulfoxide) was added to the cells until a final concentration of 0.2 nmol/L. The cells were incubated for 10 min at 37°C and then centrifuged for 5 min at 1600*g*. After discarding the medium, cells were washed once with D-PBS (Gibco/Life Technologies).

Apoptosis induction and viability measurement

MSCs at 70–80% confluency were induced to apoptosis by addition of Staurosporine, actinomycin D, MG-132 or camptothecin (Sigma), all at a final concentration of 5 μmol/L. As a reference control, staurosporine was added to a cell aliquot 24 h before mouse transplantation experiments. The ratios of dead, apoptosis-induced and live cells were determined using annexin V antibody (Becton, Dickinson and Company), propidium iodide (Becton, Dickinson and Company), caspase 3/7 activation (FLICA apoptosis detection kit, Immunochemistry Technologies), BrdU staining (Sigma Aldrich) and TMRM signal intensity loss on BD FACSCanto/LSRFortessa (BD Biosciences).

Flow cytometry

Surface marker expression was analyzed in single cell suspensions after detachment of MSCs from the bottom of the culture flask using StemPro Accutase (Gibco/Life Technologies). Cell suspensions were prepared in D-PBS for extracellular staining. Cells ($0.1–1 \times 10^6$) were incubated at 4°C for 25–30 min using directly conjugated hABs against (all Becton, Dickinson, and Company unless otherwise noted) CD105 (clone 266, FITC), CD90 (clone 5E10, APC), CD73 (clone AD2, PE), CD71 (clone MA-712, PE), CD49d (clone A9F10, APC), CD45 (clone 2D1, PE) CD44 (Miltenyi Biotec; clone DB-105, FITC), CD34 (clone 2D1 APC), CD31 (clone L133.1, APC), CD29 (clone Mar-4, PE), CD14 (clone MφP9, PE), CD11a (clone G25.2, PE) and HLA(A/B/C) (clone DX17, PE) or directly conjugated mABs against CD31 (clone MEC 13.3, APC), F4/80 (ABD Serotec; clone A3-1, Pacific Blue), GR-1 (clone RB6.8c5, APC) or indirectly labeled mAB against C3b (Thermo Scientific; clone MA1-70054) or hAB Calreticulin (Sigma-Aldrich; clone TO-11) in combination with Alexa Fluor 488 (Invitrogen; clone 15-HCLC). The samples were analyzed on BD FACSCanto or LSRFortessa and analysis performed using FACSDiva software (BD Biosciences). Graphical revision was performed using FCS Express and FlowJo 7.6.1 software.

Size determination with calibrated microbeads

Quantity and size of MSCs were determined in single cell suspensions using quantibead-dotplot analysis on BD FACSCanto and BD LSRFortessa. Size calibration performed on FACSCanto was achieved with 10-μm and 15-μm diameter calibrated latex microspheres (Invitrogen) and 29.6-μm and 66.1-μm diameter Sphero blank calibration particles (Spherotech). Size determination on BD LSRFortessa was done with calibrated ready diluted (1:1000) polystyrene microparticles (Kisker Biotech) with average diameters of 10, 16.6, 33.1, 43.6 and 66.1 μm. Average size was correlated to the respective forward scatter values. Osmolarity of control solution NaCl 0.9% with 286 mOsmol/L and pH 7.4 and D-PBS with 308 mOsmol/L and pH 7.4 was considered equivalent, and size-related differences were not measured.

Cytotoxicity assay

To detect xenogenic reaction of murine immune cells and human MSCs, a standard calcein assay was applied *in vitro* as previously described [16]. Fresh splenocytes were pooled from spleens of three C57BL/6 mice. Splenocyte viability was assessed using 0.4% trypan blue staining and during flow cytometry analysis via costaining of 7-AAD. MSCs were stained with Calcein-AM (Sigma) using 2-μmol/L calcein stock solution according to the manufacturer's protocol. Calcein-stained MSCs and splenocytes were suspended in DMEM/20% FCS. Cells were analyzed by flow cytometry 2 and 6 h after addition of splenocytes. To distinguish cell populations, splenocytes were stained with murine CD45 (APC), and the $CD45^-$ population was gated to assess Calcein-AM signal intensity of MSCs.

Quantitative polymerase chain reaction

To determine absolute MSC numbers per tissue sample, genomic DNA was isolated from defined numbers of human male MSCs using a DNeasy Blood and Tissue Kit (Qiagen). A standard curve ranging from 12 cell equivalents per microliter to 60 000 cell equivalents per microliter was prepared for quantification. Numbers of MSCs per organ were calculated from the results of DNA extracted from whole organs

using this curve and expression of the sex-determining region Y (*SRY*) in the transplanted male MSCs. DNA was analyzed using FAM/Sybr probes, forward 5′ACGAAAGCCACA-CACTCAAGAA′3 and reverse primer 5′GTGAGCTGG-CTGCGTTGAT′3 and fluorophoric probe FAM-AGCACCAGC-TAGGCCACTTACCGCC-TAMRA (Applied Biosystems). Samples were prepared in a 96-well plate on ice, working with "ready-for-use" Mastermix (Applied Biosystems). Quantitative polymerase chain reaction (qPCR) analysis was run on Applied Biosystems 7900HT Fast Real Time PCR System using Sequence Detection System Software v2.4.1, which generated amplification plots for ΔCT evaluation to extrapolate standard curve CT-value to determine cell quantity.

Animal procedure and handling

All animal procedures were approved by the local animal care facility (Central Research Association/Zentrale Forschungseinrichtung Frankfurt) and regional authority (Regierungspräsidium Darmstadt). All procedures have been defined in the animal experimentation motions TV 27/16 and TV 27/20. Eight-week-old female C57BL/6 mice (Janvier Labs) were kept under the standard animal care conditions and rested for at least 1 week before entering experimentation. Nine- to 14-week-old mice were used for all experiments. Mice were restrained in a tube restrain device without being anesthetized. A 26-G Needle (B. Brown) was inserted, after location of the vein on one side of the tail slightly distally. MSCs (2×10^6) were routinely injected in 300 µL 0.9% NaCl or HyperHAES mixed with NaCl in a 1:1 ratio. Organs were harvested after general anesthesia by exposure to saturated atmosphere of isoflurane (Baxter) after cervical dislocation. Immediately after, ~ 150 µL of blood was drawn from the heart using a 1-mL syringe and 26-G needle pre-flushed with 0.5 mol/L ethylenediaminetetraacetic acid. Subsequently, heart, lung, liver, both kidneys and spleen were prepared as previously described [17]. For workup of gut, approximately 0.2 g of gut between small intestine and colon was excised and the gut content removed. Harvested organs were directly placed on dry ice for DNA isolation or placed in ice cold D-PBS supplemented with 10% FCS for subsequent mincing and flow cytometric analysis. Mincing was done using Falcon Cell strainers (Fisher Scientific) with 70-µm grid.

Isolation of genomic DNA from murine tissues

Whole murine heart, spleen, liver, both kidneys, lungs, gut, tibiae and femurs were prepared from mice and placed on dry ice. Mouse blood was drawn into a 1-mL syringe preflushed with 0.5M EDTA (Sarstedt) and lysed by red cell lysis buffer (Sigma Aldrich). Frozen tissues were homogenized using a mortar and pestle. DNA separation steps were performed according to the DNeasy Blood and Tissue-protocol (Qiagen). Samples were dried in a vacuum Eppendorf Concentrator 5301 at 56°C until all fluid evaporated. DNA was re-suspended in 10-µL nuclease free water, and DNA concentration and purity were determined using NanoDrop (Thermo Scientific).

Isolation of genomic human DNA from MSCs

Cultured MSCs were harvested from culture flasks (5×10^6 cells per isolation). DNA separation steps were performed according to DNeasy Blood and Tissue-protocol (Qiagen). Samples were dried in a vacuum Eppendorf Concentrator 5301 at 56°C until all the fluid evaporated. DNA was re-suspended in 10 µL of nuclease-free water, and concentration and purity were determined using NanoDrop (Thermo Scientific).

Statistics

Statistical evaluation of data was performed using unpaired Student's *t*-test for analysis of parametric distributions, Mann-Whitney *U* test for analysis of unparametric distributions, and Kruskal-Wallis test for comparison of multiple groups of unparametric distributions using GraphPad Prism Version 5.0 software. Statistical tests used are indicated in the respective figure legends.

Results

Changes in morphology and surface expression in the early stage of in vitro expansion of bone marrow–derived MSCs

Culture-expanded MSCs have been described as relatively large cells that accumulate in the lungs as a first pass effect and can potentially obliterate blood vessels after intra-arterial injection [18–20]. We hypothesized that the size of MSCs might play a role in the biodistribution after systemic administration. To analyze differences in cell size during *in vitro* expansion, we first analyzed human MSCs by flow cytometry and bright field microscope during several passages in culture. MSCs form five donors were used throughout the study, which are characterized in Supplemental Figure S1. To determine the size of MSCs, calibrated ceramic microbeads of defined diameters were employed [18–20]. MSCs revealed a significant increase in average size over six culture passages (Figure 1). At passage (P)1, the mean diameter was 31.9 ± 2.02 µm, whereas MSCs at P5 (~4–5 weeks old) showed a significantly increased diameter of 42.0 ± 2.02 µm (Figure 1A,B) and also appeared as larger cells in the bright field analysis compared with P1 (Figure 1C,D). Next, MSCs were quantified and grouped into different cell diameter

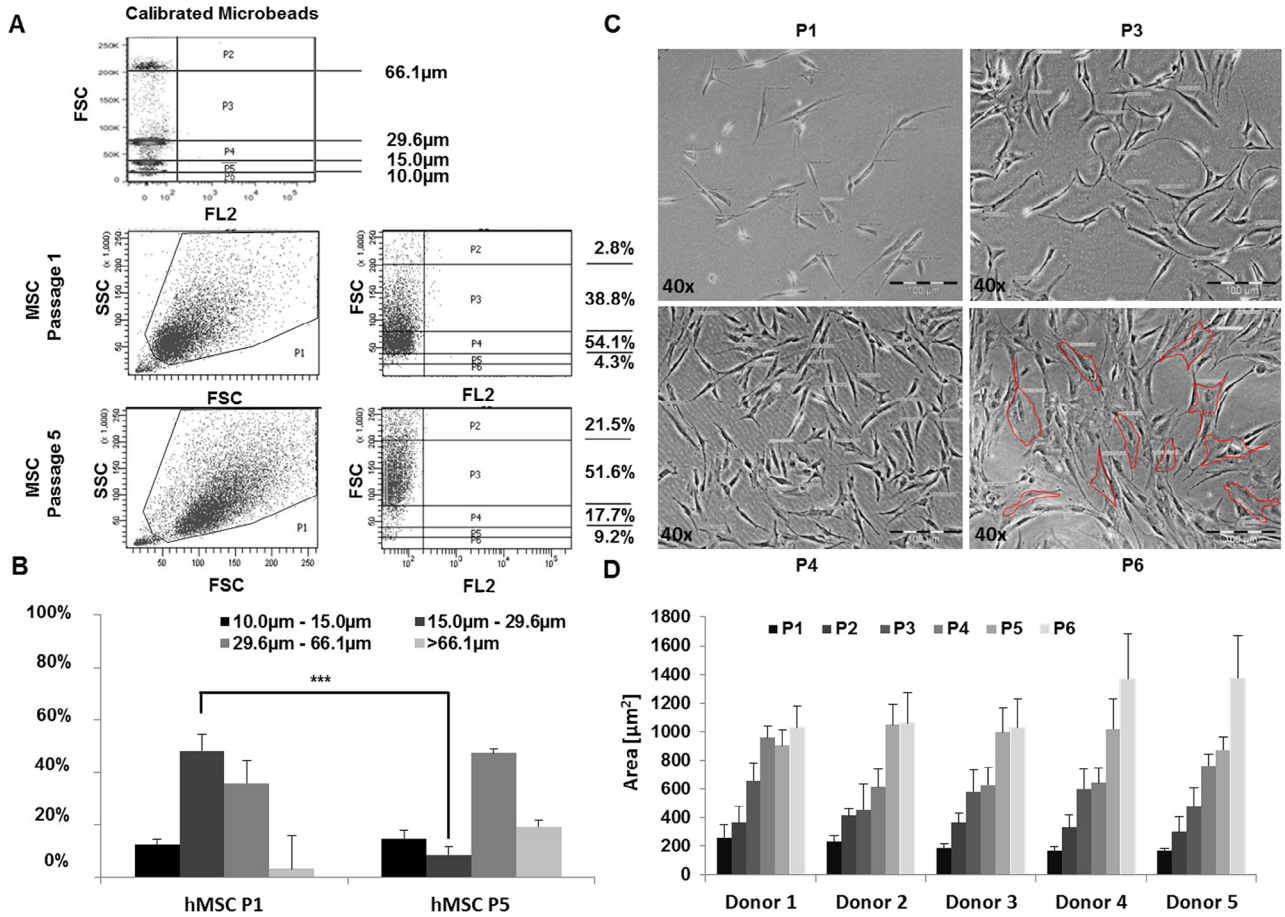

Figure 1. Changes in the size of MSCs during *in vitro* expansion. MSCs were analyzed via bright field microscopy or flow cytometry at P1 to P6. (A) Size distribution was determined via flow cytometry using calibrated ceramic microbeads ranging from 10.0 to 66.1 µm to correlate forward scatter (FSC) value to cell diameter. (B) Quantitative size distribution of isolated MSCs in P1 and P5 (means ± SD; n = 5). (C) Microscopic bright field analysis visualized morphological changes in area covered by cells during *in vitro* expansion. Cell areas were determined using red marking as indicated. (D) Quantification of cell area was performed by analysis of 150 cells per point. ***$P < 0.0001$. Statistic significance was assessed using unpaired Student's *t*-test.

classes. Early passage MSCs were mostly contained within a size group of ≤29.6 µm, whereas MSCs at later passages displayed increasing proportions of cells with diameters of ≥29.6 µm (Figure 1B). To assess changes in total area of plastic adherent MSCs, 150 randomly selected cells were analyzed at four passages by light microcopy (Figure 1C). The mean surface area at P1 was 202 ± 42 µm^2, increasing to a mean of 1171 ± 182 µm^2 at P6. This corresponds to a gain in surface area of 217.2 µm^2 per passage, and an approximately five- to six-fold increase of cell area within a time period of 40 days (Figure 1D).

Transplantation of PKH67-labeled male MSCs into female C57BL/6 mice results in loss of traceability via genomic DNA and loss of nuclei in PKH+ MSC cells

Figure 2A outlines the mouse transplantation experiments. To address the biodistribution of transplanted MSCs using MSC-specific genomic DNA, we injected 2×10^6 MSCs from male donors and studied the presence of the human *SRY* gene within murine tissue. MSCs from five donors were used in the five replicate experiments. To trace transplanted cells by flow cytometry, MSCs were labeled using a lipophilic PKH67 membrane staining dye before transplantation. To determine MSC numbers in murine tissues using quantitative analysis by human *SRY* DNA, transplanted mice were sacrificed either before or at four time points after MSCs transplantation following tissue preparation (Figure 2B). Five minutes after transplantation, the majority of human DNA signal (representing 52.5% of initially injected cells) was found in lungs and only a minor portion (0.78%) in the heart and minute amounts (representing <0.1% of injected cells) in other tissues. Human DNA signal detected in the lungs rapidly decreased to <0.1% of injected cells within 24 h (Figure 2B). At 30 min, 0.03% of the transplanted cells were found in the liver, increasing to 0.05% after 2 h and becoming

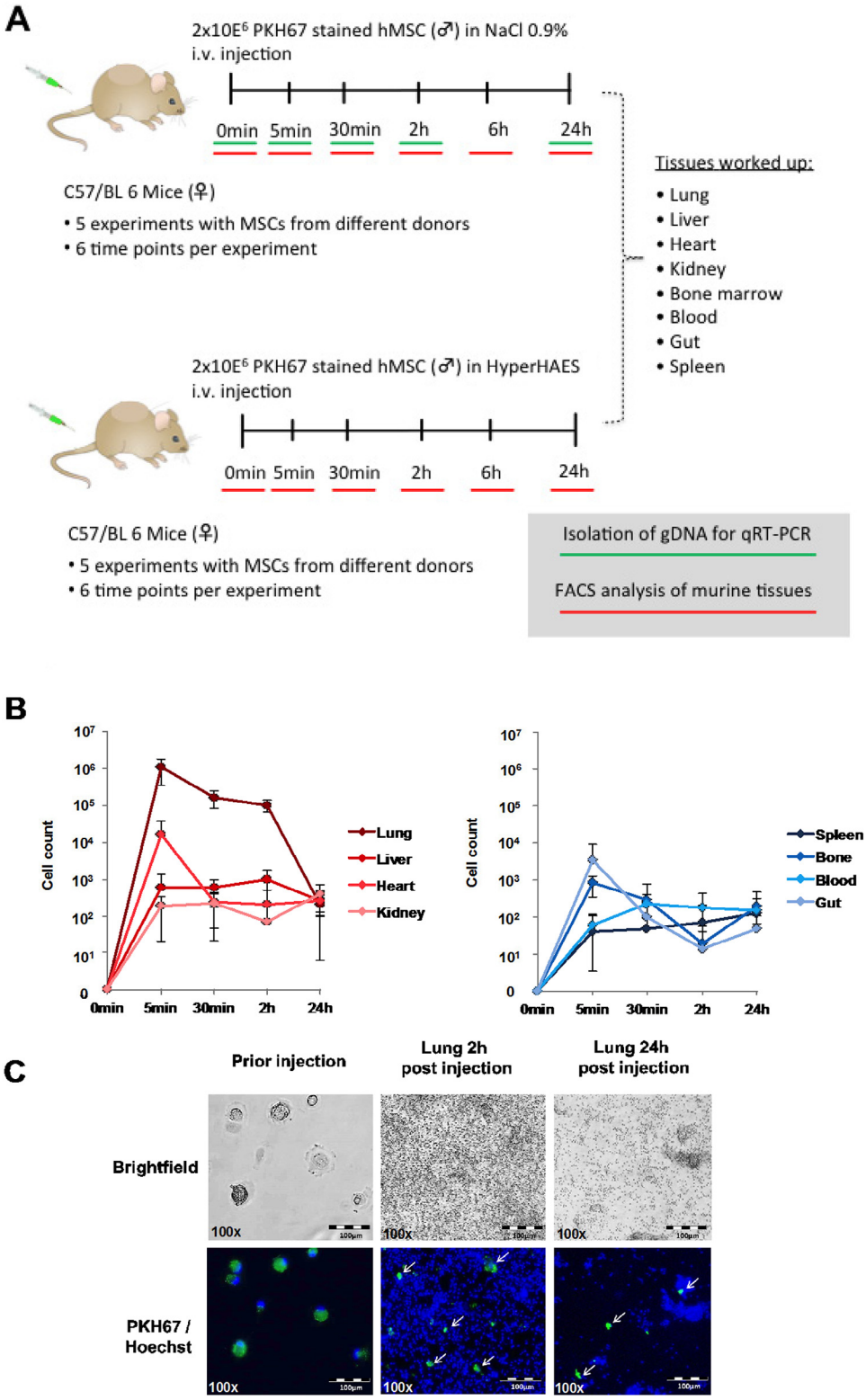

Figure 2. Experimental scheme of mouse transplantations and tracking of male PKH67-labeled male human MSCs. (A) Layout of mouse transplantation experiments. (B) Quantification of transplanted human MSCs in tissues by qPCR. Five mice per time point were injected with 2×10^6 human MSCs (Passage ≤ 5) into the tail vein and sacrificed at different time points. Copies of the human *SRY* gene were quantified in whole snap-frozen tissues by qPCR analysis. Values represent means ± SD of five independent experiments using MSCs from different donors. (B) PKH67 labeling with nuclear costaining revealed transplanted MSCs with decreased diameter and no visible nuclei (indicated by white arrows) 2 and 24 h after injection compared with MSCs before injection.

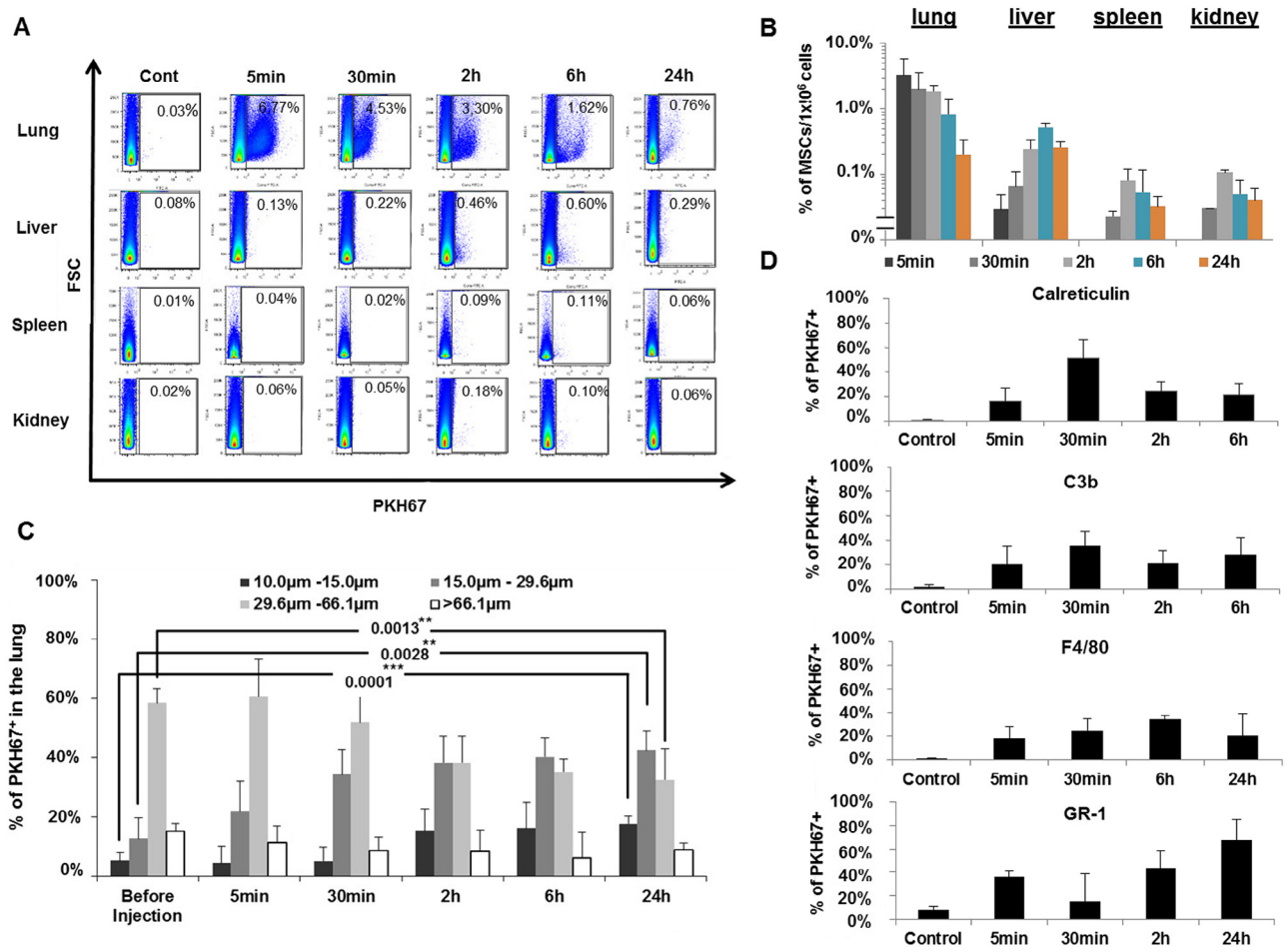

Figure 3. Determination of biodistribution, cell diameter kinetics and possible immune cell interaction of human MSCs in C57BL/6 mice. (A) Flow cytometric determination of PKH$^+$ events representing injected MSCs in different tissues at observed time points. (B) Quantitative distribution of injected MSCs in different organs by PKH67 staining. (C) Quantitative analysis of cell diameters of PKH67$^+$ events representing injected MSC in the lungs at different time points after transplantation. (D) Co-occurrence of PKH67 label and leukocyte and phagocyte cell surface markers after injection of PKH67$^+$ MSC in the lungs of transplanted mice. Bars represent mean ± SD of five experiments with MSCs from different donors. $^{**}P < 0.005$ by Mann-Whitney *U* test and Kruskal-Wallis test.

undetectable after 24 h. No more than 0.1% of injected MSCs were traced in any other tissue or time point (Figure 2B). We next tracked injected MSCs *in vivo* using PKH67 fluorescence. Before injection, microscopic analysis showed intact green fluorescent MSCs with a homogenous size distribution and intact nuclear staining, whereas fluorescencing MSCs found in the lungs of transplanted mice appeared much smaller (Figure 3C). Counter-staining using Hoechst 33342 revealed that a nuclear signal was mostly absent in PKH$^+$ MSCs after transplantation (Figure 2C). Taken together, these data indicate that most MSCs are no longer intact shortly after transplantation. To evaluate whether a xenogeneic response might influence MSCs after transplantation into immune competent mice, MSCs as the potential target were stained with Calcein-AM and their viability was assessed in the presence and absence of murine splenocytes as effector cells *in vitro* (Table I).

Table I. Cytotoxicity assay to determine potential alterations in MSC viability by immune cells.

	MSC control	MSC + splenocytes	*P* value between control and splenocytes group
0 h	41198 ± 7003		
2 h	13389 ± 2689	13633 ± 2951	0.4274
6 h	2977 ± 675	2838 ± 644	0.2795

Ten to the fifth MSCs were stained with calcein and suspended in culture medium as described in materials and methods. Next, 5×10^5 splenocytes or medium alone were added and cells were incubated for 2 and 6 h. Cell suspensions were then analyzed by flow cytometry and viability was expressed as mean signal intensities. Analyses were performed in triplicate with each replicate with MSCs from a different donor. Values are means ± SD. *P* values were calculated through two-sided Student's *t*-test. Shown is one representative out of three independent experiments, yielding comparable results.

Comparison of the calcein signal in MSCs revealed decreased mean fluorescence intensity over time, as shown previously [18]. No difference was observed between MSCs incubated in either the presence or absence of splenocytes (Table I).

Biodistribution, reduction in size and opsonization of transplanted MSC

We next analyzed the distribution and size of PKH-labeled MSCs in transplanted mice. Before injection, PKH staining efficiency was 89.0 ± 10.1%, and MSCs showed an average cell diameter of 42.2 ± 2.1 µm (means ± SD; data not shown in figure). Flow cytometric detection revealed no PKH^+ signals in tissues of non-transplanted mice (Figure 3A). Five minutes after transplantation, the highest frequencies of $PKH67^+$ events were found in the lungs (3%), and smaller percentages in the liver, spleen and kidneys. The values continuously decreased in the lungs over 24 h. Values peaked at 0.5% in liver and at about 0.1% in spleen and kidneys and then declined (Figure 3B). After 24 h, 0.2 ± 0.1% of injected cells were found in the lungs and 0.26 ± 0.05% in the liver. These are significantly higher percentages than in the kidneys 0.04 ± 0.02% and spleen 0.03 ± 0.01% ($P = 0.0147$ for lungs and $P = 0.0128$ for liver compared with spleen and kidney with unpaired *t*-test). No PKH^+ signals were found in blood, heart, bone marrow or gut, with the exception of heart at the 5-minute time point (0.03 ± 0.05%; not shown).

Next, a kinetic analysis of MSC diameters in the lungs after addition of calibrated microbeads to the samples revealed significant changes in the distribution of MSCs size compartments. Cells with a diameter between 29.6 and 66.1 µm decreased about two-fold, over 24 h, whereas the percentage of cells between 10 and 29.6 µm increased more than three-fold (Figure 3C). To investigate whether MSCs may interact with host-derived blood cells, we analyzed PKH fluorescence after co-staining of lung cell suspensions with fluorescence-labeled antibodies against markers of innate immune cells. Within 30 min after injection, more than half of the $PKH67^+$ population showed co-expression of calreticulin, a marker that serves as signal for the host immune system to consecutively induce phagocytosis (Figure 3D). At later time points, calreticulin expression in PKH^+ MSCs decreased. Furthermore, PKH^+ MSC events co-stained with antibody against complement component C3b, the macrophage marker F4/80 and the granulocyte marker GR-1 at increasing percentages over time (Figure 3D). These data indicate an interaction of transplanted MSCs with phagocytic cells early after injection.

Influence of HyperHAES on morphology and viability of MSCs

To investigate whether reducing the size of the MSCs before injection may influence their biodistribution, MSCs were preincubated in hyperosmolaric HyperHAES before transplantation. We observed a denser signal of membrane-associated actin and shrinking MSCs diameter in adherent and suspension cultures in the presence of HyperHAES compared with controls when analyzed by fluorescence microscopy, but no visible signs of DNA condensation or DNA fragmentation (Figure 4A). We next performed serial dilutions of MSCs in single cell suspensions in mixtures of HyperHAES and NaCl 0.9% at different ratios (Figure 4B). We observed that a 1:1 ratio was sufficient to reduce the cell diameter of MSCs significantly, with a decrease from 53.0 ± 4.0% to 32.2 ± 1.8% in the most frequent size-compartment of MSCs (43.6–66.1 µm; Figure 4B). This effect was only slightly enhanced at higher ratios or in pure HyperHAES. The average cell diameter of the MSCs preincubated in isotonic NaCl was 48.7 µm, which was reduced to 38.3 µm in a 1:1 ratio of HyperHAES/NaCl (Figure 4C).

Changes in the biodistribution of transplanted MSCs using HyperHAES

To detect potential changes in biodistribution after incubation of MSCs in HyperHAES or NaCl 0.9% in immune competent mice, cell suspensions from different tissues of transplanted mice were analyzed by flow cytometry. As shown in Figure 5A, in the lung, the smaller-sized PKH^+ cells increased (15–29.6 µm, from 10 to 40%; 10–15 µm from 1–5% to 10–20%) over time, whereas the larger-sized cells decreased accordingly (Figure 5A). No overt differences were noted between both treatment groups; pre-incubation in HyperHAES resulted in a somewhat higher proportion in the 29.6- to 66.1-µm-size group, and a small reduction in the 10- to 15-µm-size group compared with the saline controls (Figure 5A). In liver, spleen and kidneys, larger percentages of PKH^+ MSCs were detected after pre-incubation in Hyper-HAES compared with controls, but this was statistically significant only in liver at 2 and 6 h (Figure 5B). In the heart, spleen and kidney, MSCs became detectable only with Hyper-HAES but not in the control group (Figure 5B). This indicates that pre-incubation in HyperHAES may support MSCs to reach these tissues more efficiently.

HyperHAES modulates the interaction of transplanted MSCs with the host immune system

Although the injected MSCs were found at higher frequencies in some tissues after HyperHAES treatment, a continuous decline of traceable MSCs was seen in

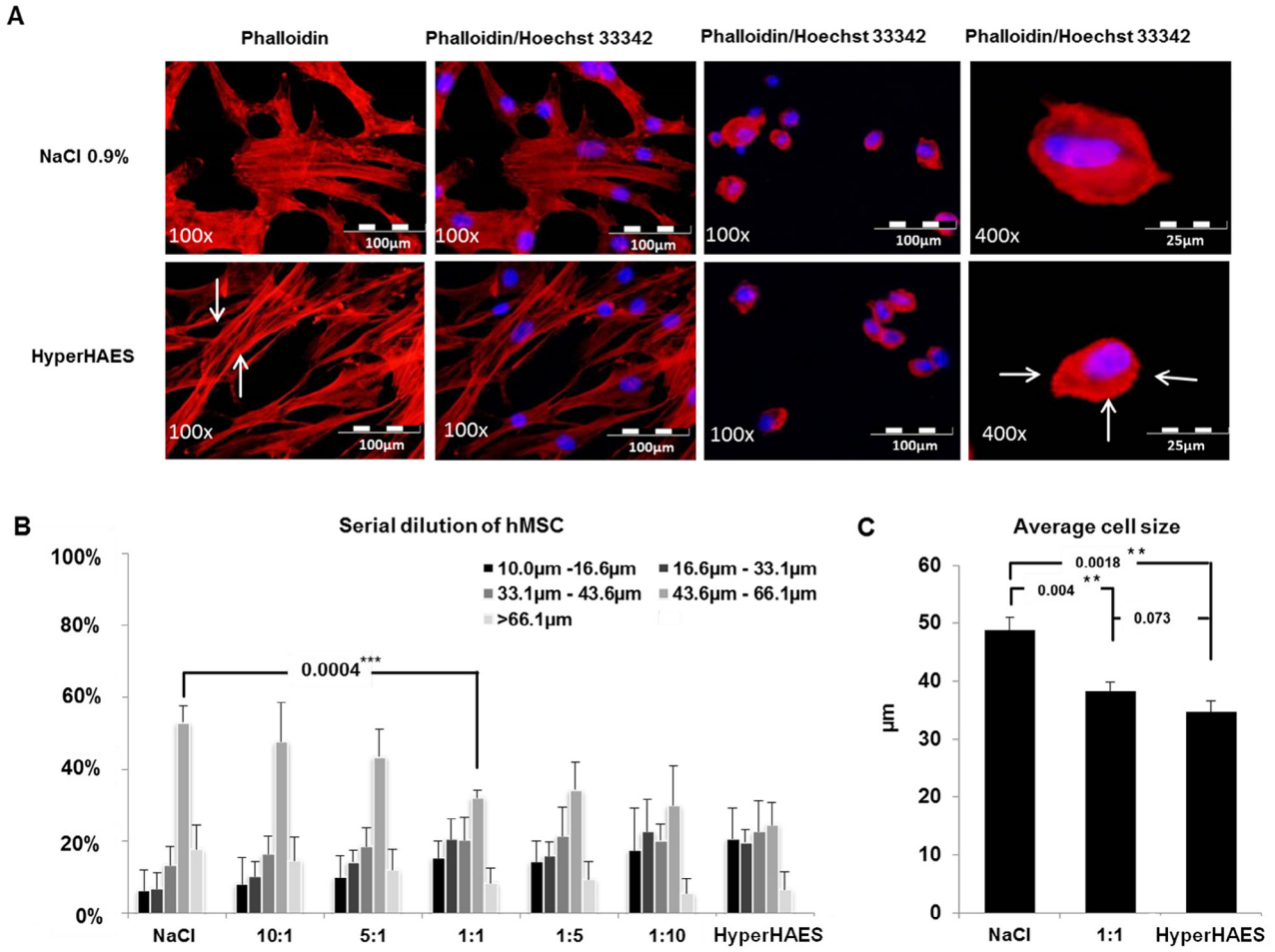

Figure 4. Influence of HyperHAES on MSC actin and cell diameter *in vitro*. (A) Phalloidin A/Hoechst 33342 staining showing actin polymerization of MSC treated with 1:1 HyperHAES/NaCl 0.9% in fluorescence microscopy. Left two panels: MSCs before trypsinization; right two panels: MSCs after trypsinization. Increased actin density is marked with arrows. The images shown are representative of three independent experiments each. (B) Relative distribution of MSC cell size groups as analyzed by flow cytometry after incubation at different ratios of HyperHAES and isotonic saline for 5 min. (C) Mean cell diameter determined of MSCs after incubation in 0.9% NaCl or HyperHAES for 5 min as analyzed by flow cytometry. Data in panels B and C represent means ± SD, n = 5 using MSCs from five donors. *$P < 0.05$; **$P < 0.005$ by unpaired Student's *t*-test. MSCs were analyzed at P4–P5.

both groups over time. To investigate potential interactions of MSCs with host cells, the co-occurrence of phagocyte antigens or a platelet-/endothelial receptor PECAM-1 on PKH$^+$ events was compared. The intensity of the calreticulin signal on PKH$^+$ MSCs increased after 30 min and then decreased after 6 h in saline control solution, whereas with HyperHAES, expression of calreticulin constantly increased over time. Co-staining of the macrophage marker F4/80, the granulocyte marker GR-1 and the endothelial and platelet marker CD31/PECAM-1 also increased time-dependently in PKH$^+$ MSCs, with little differences between both groups (Figure 6B,C). CD90 remained present on nearly all PKH$^+$ events, whereas CD73 expression constantly decreased, which is consistent with the observed decline of CD73 in apoptosis-induced MSCs in culture. No major systematic differences were observed between the treatment groups for these markers. HLA(A/B/C) was found to be only marginally expressed in transplanted tracked MSCs (Figure 6C).

Modulation of viability and mitochondrial integrity in MSCs preincubated with Hyper-HAES

To analyze whether pre-incubation with HyperHAES may positively influence the viability of injected MSCs, several viability markers were investigated in transplanted MSCs using co-staining with PKH. First, the efficiency of several apoptosis inducers to induce apoptosis in MSCs was tested *in vitro*. Staurosporine proved to be the most potent apoptosis inducer for MSCs with

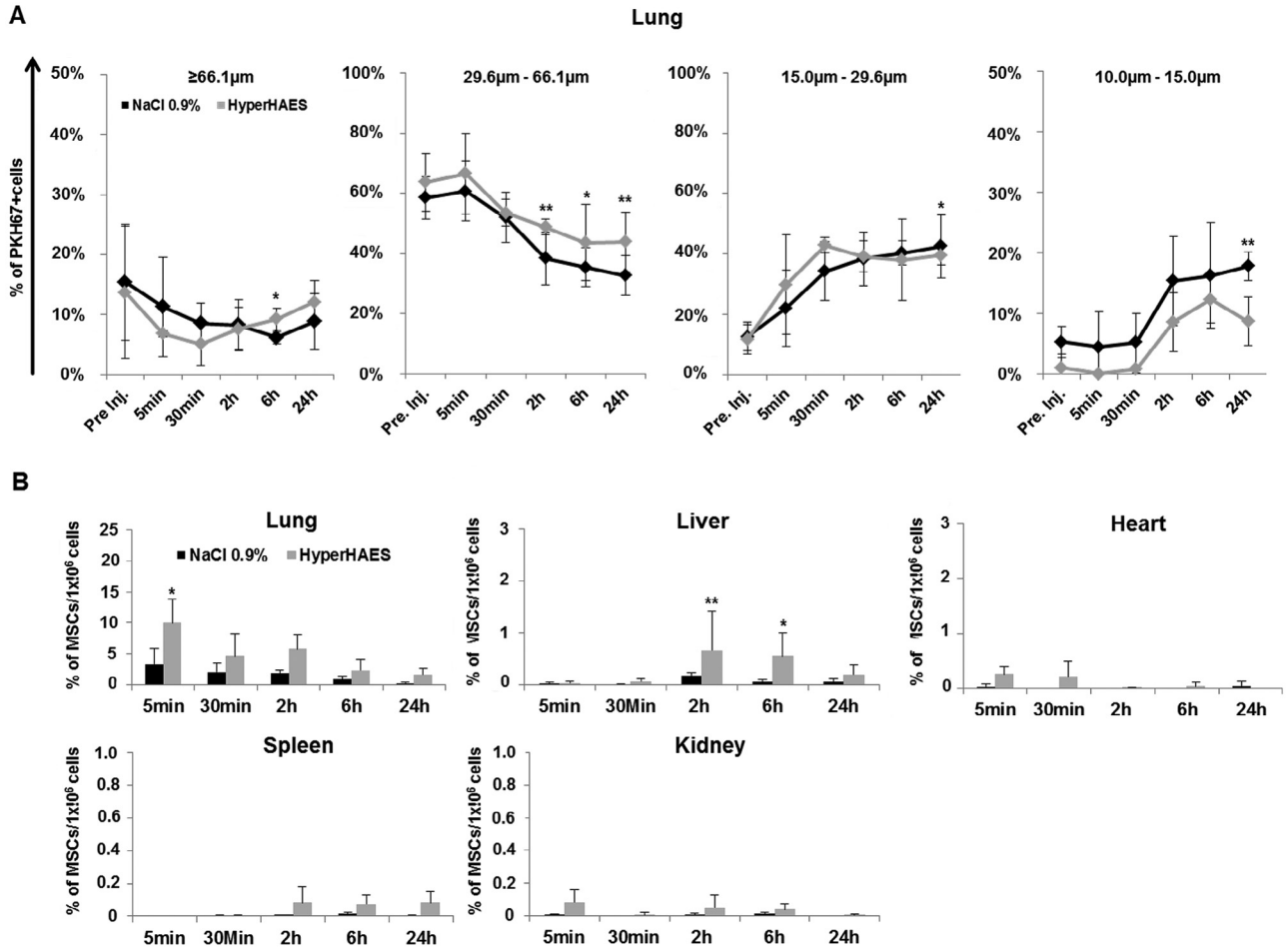

Figure 5. Cell diameter and biodistribution of injected MSC in different tissues after transplantation in immune competent mice. (A) Quantitative analysis of the distribution of PKH67 positive events representing different cell diameters of injected MSC in NaCl 0.9% and HyperHAES. (B) Isolation and analysis of murine tissues after injection of NaCl 0.9% or HyperHAES preincubated MSC. Shown are values obtained from lungs, liver, heart spleen and kidney; $PKH67^+$ events were not detectable in gut, blood and bone marrow in all groups (not shown). Bars represent means ± SD, n = 5 experiments with MSCs from different donors. $*P < 0.05$; $**P < 0.001$ by Mann-Whitney *U* test.

close to 75% apoptosed/dead cells after 24 h, although it proved less efficient than in other cell lines like Jurkat or HeLa (26;27). After 24 h of incubation with staurosporine, only a small percentage of MSCs remained viable, while cell shrinkage and membrane blebbing was observed in the majority of MSCs (Figure 7A). Staurosporine was therefore used to survey the inducibility of apoptosis in the different *in vivo* experiments. Next, detection of changes in mitochondrial membrane potential was established using TMRM staining. Apoptosis-induced MSCs were used as a reference population and showed a mean signal loss of more than 70.2 ± 10.7%. Shortly after transplantation of (non-induced) $PKH67^+$ MSCs, the TMRM signal of saline-preincubated MSCs in the lungs was even lower than the apoptosis induced signal *in vitro* (Figure 7B). Compared with saline-incubated MSCs, HyperHAES pre-incubated MSCs showed better preservation of mitochondrial integrity and higher TMRM signals for up to 6 h (Figure 7B).

Analysis of additional markers for apoptosis and cell death in PKH^+ MSCs post-transplantation revealed comparable increases of the annexin V binding signal in both groups, with slightly lower annexin V signals in HyperHAES after 24 h (Figure 7C). In contrast, propidium iodide signal intensity was higher with saline controls than with HyperHAES MSCs over the first 6 h, and later became similar (Figure 7C). Activation of caspase-3/7 was also observed in both groups. In the first 5 min post-transplantation, the caspase activity was significantly lower with HyperHAES, but the difference was not statistically significant over time (Figure 7C). In conclusion, apoptosis markers are generally increasing on traced MSCs in our transplantation model. Preincubation of MSCs with Hyper-HAES could preserve mitochondrial

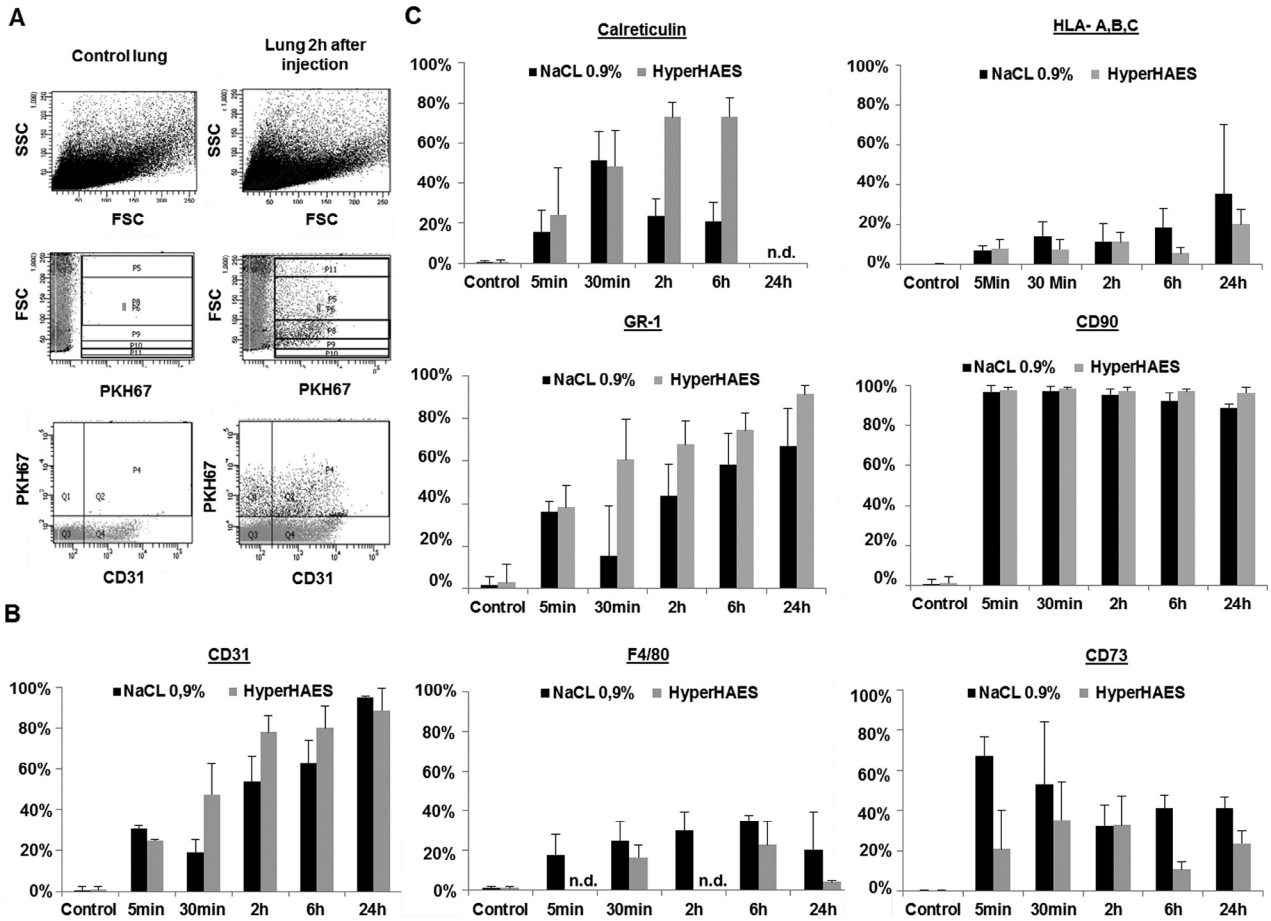

Figure 6. Co-occurrence of leukocyte antigens and PKH$^+$ MSC signal after injection of MSC preincubated in NaCl 0.9% or HyperHAES and transplanted in immunocompetent mice. PKH67$^+$ events were tracked in a FSC/SSC leukocyte gate by flow cytometry. (A) Representative scatter plot and fluorescence gating strategy is shown for a control and a test mouse with costaining of murine CD31. Signal intensity was determined by Q2/Q1 ratio (P4 gate). Panels B and C: analysis after co-staining with antibodies recognizing MSC, immune cell or platelet/endothelial markers. Bars represent means ± SD of four to six independent experiments using MSCs from different donors. $^*P < 0.05$, $^{**}P < 0.005$ and $^{***}P < 0.0005$ by Mann-Whitney *U* test. n.d., not determined.

integrity and reduce propidium iodide influx into transplanted MSCs.

Discussion

In this study, we investigated the fate of bone marrow–derived MSCs after systemic administration in immunocompetent mice. We compared tracing of MSCs using a specific DNA marker and the membrane dye PKH67 and calibrated microbeads. In addition, we compared iso- and hyperosmolar injection medium. Our data demonstrate a rapid reduction in the size of transplanted MSC, as well as loss of cell nuclei and DNA. Moreover, we demonstrate fragmentation of MSCs, acquisition of opsonization signals and detection of phagocyte surface markers on transplanted MSCs. Together our data reveal a role of fragmentation in the fate of intravenously injected MSCs and help to explain the decreased traceability of transplanted MSCs in many preclinical models.

qPCR analysis revealed rapid loss of traceable human DNA within the first 24 h after systemic administration. Intriguingly, microscopic analysis using nuclear counterstaining of MSCs in the lungs showed that nuclei were also rarely visible in PKH$^+$ cells early after injection. In addition, we found induction of apoptosis markers on MSCs. This indicates a loss of MSCs nuclear and cellular integrity at early time points during circulation or lung passage. Moreover, transplanted MSCs were detected by flow cytometry and PKH$^+$ marker at higher frequencies throughout the analyzed tissues than by qPCR. Loss of DNA in PKH$^+$ MSCs or their fragments was confirmed by fluorescence microscopy. It remains an open question whether the observed low-diameter cells that were tracked by polystyrene microbeads were osmotically altered MSCs or fragments of MSCs generated by mechanical disruption [21–23].

Transfer of the lipophilic membrane dye PKH67 from MSCs to other cells might theoretically also result

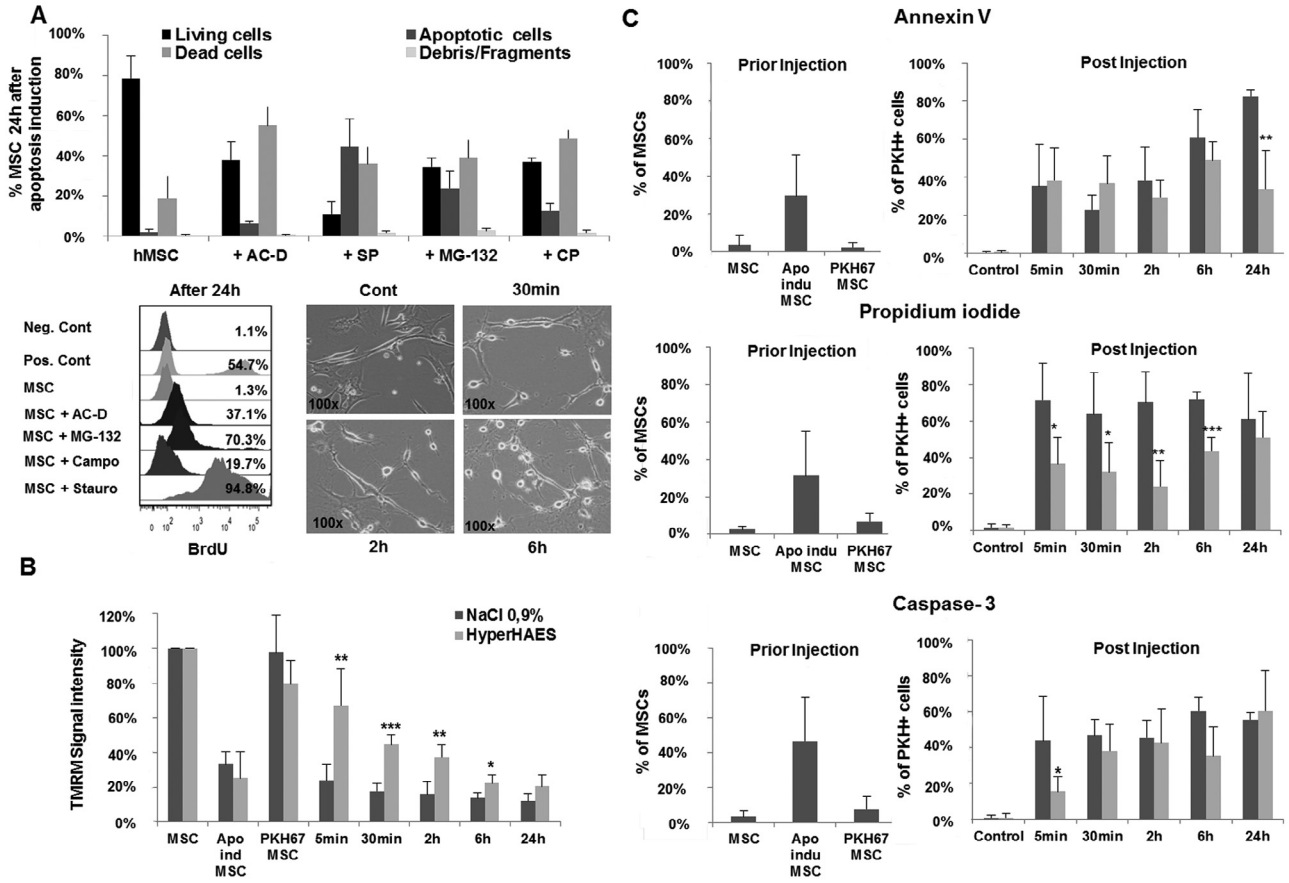

Figure 7. Loss of mitochondrial membrane potential and increase of apoptosis markers of MSCs after transplantation in mice. (A) *In vitro* apoptosis induction of MSC using different stimuli analyzed by flow cytometry (upper panel and left) or light microscopy (lower right). MSCs were incubated for 24 h. (B) Signal intensity of TMRM increment in transplanted PKH67$^+$ MSC was determined by flow cytometry in the lungs 24 h after injection. (C) Comparison of viability signals of injected PKH67$^+$ MSC preincubated and injected with NaCl 0.9% and HyperHAES at different time points after transplantation. The bars in panels B and C represent means ± SD; n = 5 experiments with MSCs from different donors. $*P < 0.05$; $**P < 0.005$ $***P < 0.0001$ by Mann-Whitney U Test. AC-D, actinomycin D; CP, camptothecin; SP, staurosporine;.

in the presence of fluorescence-signals in host cells. However, in this study, we observed a co-occurrence of PKH fluorescence with markers in murine cells within minutes to a few hours after transplantation, whereas the previous reports [24–26] demonstrated that the transfer of PKH label requires much longer time periods, from a few days to several weeks. We cannot, however, rule out that at least part of the observed PKH fluorescence in murine cells resulted from MSCs that shed small particles, for example, microvesicles that could be taken up by host phagocytes (Gr-1, F4/80 co-labels) or platelets/endothelial cells (CD31 co-label). A direct interaction of MSCs with host cells was confirmed using human MSCs tracked in C57/BL6 mice by intravital microscopy [27], observing that intravenously administered MSCs interact *in vivo* with clusters of platelets and neutrophils.

A combination of cell viability markers annexin V, propidium iodide, caspase activation and mitochondrial membrane potential was used to elucidate whether the decline in traceability of transplanted MSCs is mediated by apoptosis induction or other processes are involved. The high propidium iodide signal in the transplanted cells early after injection, in combination with a rapid decrease in mitochondrial membrane potential, indicates a fast and robust impact on injected MSCs after administration, rather than a time-dependent coordinated induction of apoptosis as seen *in vitro* [28,29]. In contrast, analysis of apoptotic markers in MSCs *in vitro* revealed that MSCs are resistant to several classical apoptosis inducers, and that apoptosis initiation required 6-18h [30]. The early induction of apoptosis in the transplanted MSCs is in line with our observation that PKH$^+$ MSCs accumulated in the liver and spleen after 2–6 h, that is, tissues where damaged or aged circulating blood cells are degraded. Previous studies have concluded that intravenously transplanted MSCs are short-lived [31,32]. Whether the observed phenomena are also associated with the generation of microvesicles and

whether this might be related to the *in vivo* effects seen in clinical trials using MSCs remains an open question and could not be answered by flow cytometry assays because of the size detection limit of ~1 μm used by the flow cell.

We deliberately used an immunocompetent mouse model in this study to be able to track potential interactions of injected MSCs with an intact host immune system. We did not observe any detectable differences in cell viability in the presence of splenocytes, indicating that at least within 6 h after transplantation, host effector cells would not avidly react to eliminate transplanted xenogeneic target MSCs. Studies in immunocompetent mice using human MSCs have also proven that xenografted MSCs could transmigrate and prove effective by influencing pneumonia healing [33–35].

The use of hyperosmolaric medium represents a novel approach in MSC therapy. Hyperosmolaric solutions should provide two beneficial effects to cell administration: First, cell shrinkage due to the high extracellular concentration of osmotically active substances surrounding MSCs before transplantation. Second, an increase in the volume of small blood vessels is expected in the transplanted host after injection of 100 μL Hyper-HAES into an estimated murine blood volume of around 1 mL, potentially increasing the blood volume and capillary diameters, enabling bigger cells to pass more easily through capillaries [36,37]. A 1:1 dilution of HyperHAES in NaCl 0.9% resulted in a decreased MSC diameter by approximately 23%. This was associated with a slower decrease in mitochondrial membrane potential, transiently greater cell viability and higher detection frequency compared with transplantation of saline MSCs. The use of HyperHAES in volume replacement therapy has been controversial because of side effects ranging from disturbance of renal function, inhibition of coagulation cascade or septic reactions in patients with trauma and burns. Patient safety and efficiency were investigated in several large trials [38,39]. Ongoing research has yet to prove the applicability of this approach to cellular therapy. HyperHAES could be used as a tool to increase MSC bioavailability after systemic administration and thus extend beneficial outcomes in research and patient treatment.

Acknowledgments

The authors thank the team members at the Institute of Transfusion Medicine and Immune Hematology, German Red Cross Blood Donor Service, University of Frankfurt, for their constant support.

This work was supported by the Deutsche Forschungsgemeinschaft and German Ministry for Education and Research (BMBF; grant SFB T/R 23) through MSC for ISLE.

Disclosure of interests: The authors have no commercial, proprietary, or financial interest in the products or companies described in this article.

References

[1] Orbay H, Tobita M, Mizuno H. Mesenchymal stem cells isolated from adipose and other tissues: basic biological properties and clinical applications. Stem Cells Int 2012;2012:461718.

[2] Dominici M, Le BK, Mueller I, Slaper-Cortenbach I, Marini F, Krause D, et al. Minimal criteria for defining multipotent mesenchymal stromal cells. The International Society for Cellular Therapy position statement. Cytotherapy 2006;8(4):315–17.

[3] Battula VL, Treml S, Bareiss PM, Gieseke F, Roelofs H, de Zwart P, et al. Isolation of functionally distinct mesenchymal stem cell subsets using antibodies against CD56, CD271, and mesenchymal stem cell antigen-1. Haematologica 2009;94(2):173–84.

[4] Buhring HJ, Battula VL, Treml S, Schewe B, Kanz L, Vogel W. Novel markers for the prospective isolation of human MSC. Ann NY Acad Sci 2007;1106:262–71.

[5] Quirici N, Soligo D, Bossolasco P, Servida F, Lumini C, Deliliers GL. Isolation of bone marrow mesenchymal stem cells by anti-nerve growth factor receptor antibodies. Exp Hematol 2002;30(7):783–91.

[6] Sethe S, Scutt A, Stolzing A. Aging of mesenchymal stem cells. Ageing Res Rev 2006;5(1):91–116.

[7] Tichon A, Gowda BK, Slavin S, Gazit A, Priel E. Telomerase activity and expression in adult human mesenchymal stem cells derived from amyotrophic lateral sclerosis individuals. Cytotherapy 2009;11(7):837–48.

[8] Stolzing A, Jones E, McGonagle D, Scutt A. Age-related changes in human bone marrow-derived mesenchymal stem cells: consequences for cell therapies. Mech Ageing Dev 2008;129(3):163–73.

[9] Son BR, Marquez-Curtis LA, Kucia M, Wysoczynski M, Turner AR, Ratajczak J, et al. Migration of bone marrow and cord blood mesenchymal stem cells in vitro is regulated by stromal-derived factor-1-CXCR4 and hepatocyte growth factor-c-met axes and involves matrix metalloproteinases. Stem Cells 2006;24(5):1254–64.

[10] Karp JM, Leng Teo GS. Mesenchymal stem cell homing: the devil is in the details. Cell Stem Cell 2009;4(3):206–16.

[11] Togel F, Cohen A, Zhang P, Yang Y, Hu Z, Westenfelder C. Autologous and allogeneic marrow stromal cells are safe and effective for the treatment of acute kidney injury. Stem Cells Dev 2009;18(3):475–85.

[12] Makela T, Takalo R, Arvola O, Haapanen H, Yannopoulos F, Blanco R, et al. Safety and biodistribution study of bone marrow-derived mesenchymal stromal cells and mononuclear cells and the impact of the administration route in an intact porcine model. Cytotherapy 2015;17(4):392–402.

[13] Honczarenko M, Le Y, Swierkowski M, Ghiran I, Glodek AM, Silberstein LE. Human bone marrow stromal cells express a distinct set of biologically functional chemokine receptors. Stem Cells 2006;24(4):1030–41.

[14] Stappenbeck TS, Miyoshi H. The role of stromal stem cells in tissue regeneration and wound repair. Science 2009;324(5935):1666–9.

[15] Teo GS, Yang Z, Carman CV, Karp JM, Lin CP. Intravital imaging of mesenchymal stem cell trafficking and association

with platelets and neutrophils. Stem Cells 2015;33(1):265–77.
[16] Somanchi SS, McCulley KJ, Somanchi A, Chan LL, Lee DA. A novel method for assessment of natural killer cell cytotoxicity using image cytometry. PLoS ONE 2015;10:doi:10.1371/journal.pone.0141074. <http://journals.plos.org/plosone/article?id=10.1371/journal.pone.0141074>; [accessed 07.10.16]. e0141074.
[17] Rüster B, Göttig S, Ludwig RJ, Bistrian R, Müller S, Seifried E, et al. Mesenchymal stem cells display coordinated rolling and adhesion behavior on endothelial cells. Blood 2006;108(12):3938–44. Epub 2006 Aug 8.
[18] Gillissen MA, Yasuda E, de Jong G, Levie SE, Go D, Spits H, et al. The modified FACS calcein AM retention assay: a high throughput flow cytometer based method to measure cytotoxicity. J Immunol Methods 2016;434:16–23.
[19] Sukerkar PA, Rezvi UG, Macrenaris KW, Patel PC, Wood JC, Meade TJ. Polystyrene microsphere-ferritin conjugates: a robust phantom for correlation of relaxivity and size distribution. Magn Reson Med 2011;65(2):522–30.
[20] van Gaal EV, Spierenburg G, Hennink WE, Crommelin DJ, Mastrobattista E. Flow cytometry for rapid size determination and sorting of nucleic acid containing nanoparticles in biological fluids. J Control Release 2010;141(3):328–38.
[21] Lassailly F, Griessinger E, Bonnet D. "Microenvironmental contaminations" induced by fluorescent lipophilic dyes used for noninvasive in vitro and in vivo cell tracking. Blood 2010;115(26):5347–54.
[22] Tario JD Jr, Gray BD, Wallace SS, Muirhead KA, Ohlsson-Wilhelm BM, Wallace PK. Novel lipophilic tracking dyes for monitoring cell proliferation. Immunol Invest 2007;36(5–6):861–85.
[23] Weir C, Morel-Kopp MC, Gill A, Tinworth K, Ladd L, Hunyor SN, et al. Mesenchymal stem cells: isolation, characterisation and in vivo fluorescent dye tracking. Heart Lung Circ 2008;17(5):395–403.
[24] Bustamante J, Caldas LE, Garcia M, Di LE, Alvarez E, Hajos SE. Disruption of mitochondrial membrane potential during apoptosis induced by PSC 833 and CsA in multidrug-resistant lymphoid leukemia. Toxicol Appl Pharmacol 2004;199(1):44–51.
[25] Denning MF, Wang Y, Tibudan S, Alkan S, Nickoloff BJ, Qin JZ. Caspase activation and disruption of mitochondrial membrane potential during UV radiation-induced apoptosis of human keratinocytes requires activation of protein kinase C. Cell Death Differ 2002;9(1):40–52.
[26] Wei H, Li Z, Hu S, Chen X, Cong X. Apoptosis of mesenchymal stem cells induced by hydrogen peroxide concerns both endoplasmic reticulum stress and mitochondrial death pathway through regulation of caspases, p38 and JNK. J Cell Biochem 2010;111(4):967–78.
[27] Furlani D, Ugurlucan M, Ong L, Bieback K, Pittermann E, Westien I, et al. Is the intravascular administration of mesenchymal stem cells safe? Mesenchymal stem cells and intravital microscopy. Microvasc Res 2009;77(3):370–6.
[28] Kraitchman DL, Tatsumi M, Gilson WD, Ishimori T, Kedziorek D, Walczak P, et al. Dynamic imaging of allogeneic mesenchymal stem cells trafficking to myocardial infarction. Circulation 2005;112(10):1451–61.
[29] Eggenhofer E, Benseler V, Kroemer A, Popp FC, Geissler EK, Schlitt HJ, et al. Mesenchymal stem cells are short-lived and do not migrate beyond the lungs after intravenous infusion. Front Immunol 2012;3:297.
[30] Monsel A, Zhu YG, Gennai S, Hao Q, Hu S, Rouby JJ, et al. Therapeutic effects of human mesenchymal stem cell-derived microvesicles in severe pneumonia in mice. Am J Respir Crit Care Med 2015;192(3):324–36.
[31] Li J, Ezzelarab MB, Cooper DK. Do mesenchymal stem cells function across species barriers? Relevance for xenotransplantation. Xenotransplantation 2012;19(5):273–85.
[32] Choi EW, Lee HW, Shin S, Park JH, Yun TW, Youn HY, et al. Comparative efficacies of long-term serial transplantation of syngeneic, allogeneic, xenogeneic, or CTLA4Ig overproducing xenogeneic adipose tissue-derived mesenchymal stem cells on murine systemic lupus erythematosus. Cell Transplant 2016;25(6):1193–206.
[33] Haase N, Muller R, Perner A. Debate on HES safety is important, but must be based on facts. Scand J Trauma Resusc Emerg Med 2013;21:66.
[34] Perner A, Haase N, Guttormsen AB, Tenhunen J, Klemenzson G, Aneman A, et al. Hydroxyethyl starch 130/0.42 versus Ringer's acetate in severe sepsis. N Engl J Med 2012;367(2):124–34.
[35] Leibacher J, Henschler R. Biodistribution, migration and homing of systemically applied mesenchymal stem/stromal cells. Stem Cell Res Ther 2016;7(1):7.
[36] Myburgh J, Li Q, Heritier S, Dan A, Glass P. Statistical analysis plan for the Crystalloid Versus Hydroxyethyl Starch Trial (CHEST). Crit Care Resusc 2012;14(1):44–52.
[37] Myburgh JA, Finfer S, Bellomo R, Billot L, Cass A, Gattas D, et al. Hydroxyethyl starch or saline for fluid resuscitation in intensive care. N Engl J Med 2012;367(20):1901–11.
[38] Thiel H, Roewer N. Anästhesiologische pharmakotherapie: von den grundlagen der pharmakologie zur medikamentenpraxis, vol. 3. Georg Thieme Verlag; 2014 ISBN 3131592834.
[39] Haase N, Wetterslev J, Winkel P, Perner A. Bleeding and risk of death with hydroxyethyl starch in severe sepsis: post hoc analyses of a randomized clinical trial. Intensive Care Med 2013;39(12):2126–34.

Appendix: Supplementary material

Supplementary data to this article can be found online at doi:10.1016/j.jcyt.2016.09.010.